European Journal of Medicinal Chemistry 66 (2013) 489–498

Contents lists available at SciVerse ScienceDirect

European Journal of Medicinal Chemistry

journal homepage: http://www.elsevier.com/locate/ejmech

Original article

Structural variations on antitumour agents derived from bisacylimidoselenocarbamate. A proposal for structure–activity relationships based on the analysis of conformational behaviour

María Font [a,*], Elena Lizarraga [b], Elena Ibáñez [c], Daniel Plano [c], Carmen Sanmartín [c], Juan A. Palop [c]

[a] Sección de Modelización Molecular, Facultad de Farmacia, Departamento de Química Orgánica y Farmacéutica, Universidad de Navarra, Irunlarrea, 1, E-31008 Pamplona, Spain
[b] Sección de técnicas instrumentales, Departamento de Química Orgánica y Farmacéutica, Universidad de Navarra, Irunlarrea, 1, E-31008 Pamplona, Spain
[c] Sección de síntesis, Departamento de Química Orgánica y Farmacéutica, Universidad de Navarra, Irunlarrea, 1, E-31008 Pamplona, Spain

ARTICLE INFO

Article history:
Received 25 March 2013
Received in revised form
31 May 2013
Accepted 1 June 2013
Available online 18 June 2013

Keywords:
Antiproliferative
Bisacylimidoselenocarbamate
Methylselenol release

ABSTRACT

A molecular modelling study has been carried out on a previously reported series of symmetrically substituted bisacylimidoselenocarbamate (BSeC) derivatives that show remarkable antitumour activity *in vitro* against a panel of human tumour cell lines. These derivatives can be considered as a central scaffold constructed around a methyl carbamimidoselenoate nucleus in which two heteroarylacyl fragments are located on the scaffold nitrogen atoms, thus forming the different BSeCs. The results reveal that the nature of the selected heteroaryl ring has a marked influence on the antiproliferative activity of the compounds and this can be related, as a first approximation, to the ability to release methylselenol (MeSeH), a compound that, according to our initial hypothesis, is ultimately responsible for the antitumour activity of the compounds under investigation. The release of MeSeH from the active BSeCs has been confirmed by means of Head Space Gas Chromatography Mass Spectrometry techniques. The data that support this connection include the topography of the molecules, the conformational behaviour of the compounds, which influences the accessibility of the hydrolysis point, the interaction map obtained for an O2H type probe, and the location and energy of the HOMO/LUMO orbitals.

1. Introduction

Among the different strategies pursued in recent years to study the factors involved in the development of tumour processes, it is worth highlighting the studies related to the true role played by some essential trace elements such as selenium (which is essential for the proper functioning of an organism but is toxic in high doses [1,2]) in cancer prevention and the possible involvement of this element in the control of processes that trigger tumour development. In fact, a substantial body of persuasive evidence indicates that selenium (Se) plays a role in cancer prevention [3–6] despite the discrepancies observed in different epidemiological nutritional studies [7–9]. These discrepancies could be related to the different chemical forms in which Se was administered to subjects involved in the studies [10]. The mechanisms underlying the influence of Se chemical forms are not yet fully elucidated – including their metabolic products, their doses and the possible involvement of different molecular targets and apparent mechanisms. However, it is commonly accepted that the three most important forms of Se in cancer prevention are sodium selenite (SS), L-selenomethionine (SeMet) and Se-methylselenocysteine (MeSeCys) [11–13]. Furthermore, there is evidence that the various forms of selenium have different capacities to induce cell death in various tumour cell lines and that this behaviour is related to Se metabolites [14–16].

As an example, methylselenol (MeSeH) has been hypothesized to be a critical Se metabolite for anticancer activity in vivo [17–19]. The biological specificity of MeSeH generation in cell culture media has been well established [20,21]. In this respect, several recent studies have shown that, in different culture media and cell lines, MeSeH generated by incubating methioninase (METase) with SeMet is responsible for anticarcinogenic effects, including regulation of gene expression [22,23]. It can be hypothesized that different signalling pathways are involved in MeSeH-induced regulation of the cell cycle and apoptosis and that these factors play a significant role in the inhibition of the invasive potential of tumour cells.

* Corresponding author. Tel.: +34 948 425 600; fax: +34 948 425 649.
E-mail address: mfont@unav.es (M. Font).

0223-5234/$ – see front matter © 2013 Elsevier Masson SAS. All rights reserved.
http://dx.doi.org/10.1016/j.ejmech.2013.06.001

In recent years, our group has developed a series of bisacylimidoselenocarbamate (BSeC) derivatives that show interesting antitumour activity [24,25] and this activity has recently been related to the ability to release MeSeH [26,27]. According to our starting hypothesis, the possibility of controlled delivery of MeSeH, achieved by means of structural variations carried out on a lead compound, makes this approach an interesting tool to develop new antitumour agents and to provide new insights into the mechanisms of the anticancer properties of Se.

In our investigations into the mechanism of action of these derivatives we have demonstrated that several of them release MeSeH under hypoxic conditions. In our previous work, *N*,*N*′-diacetyl-2-methylisoselenourea (I, Fig. 1) was selected as a lead compound and this is the simplest derivative from a structural viewpoint. This compound showed the most intense and rapid release of MeSeH of the tested BSeCs and we subsequently designed new derivatives in which the molecular architecture became progressively more complicated as a consequence of the replacement of the lateral methyl groups by aromatic or heteroaromatic rings (II, Fig. 1). The aim of these modifications was to modulate the speed and intensity of the MeSeH release, taking into account the kinetics of this liberation, which were found to be highly dependent on the nature of the lateral rings and the type, size and location of substituents on these rings and correlated with their proven pro-apoptotic activity [25,26].

Taking into account the data previously obtained in the first design cycle (Fig. 1a), in the work described here we carried out a molecular modelling study on the new BSeCs corresponding to the second design cycle (Fig. 1b). The compounds can be considered to consist of a central scaffold constructed around a methyl carbamimidoselenoate in which two heteroarylacyl fragments are located on the scaffold nitrogen atoms. The lateral heteroaromatic rings (monocyclic, bicyclic and tricyclic rings) were chosen in order to cover a wide range of electronic properties (pi-deficient, pi and pi-excessive systems), surface and volume. The aim was to evaluate the ability of these features to modulate the release of MeSeH. In this way, the whole imidoselenocarbamate is considered as a prodrug and the heteroaromatic moieties as the release regulator elements. According to the proposed mechanism (Fig. 2), hydrolysis can be mediated by the nucleophilic attack of a water molecule on the carbon that supports the methylselene fragment.

The cytotoxic activities of the analysed compounds were reported previously [24,26]. The GI_{50} value (i.e. the dose that inhibits 50% of cell growth) was considered as a cytotoxic parameter

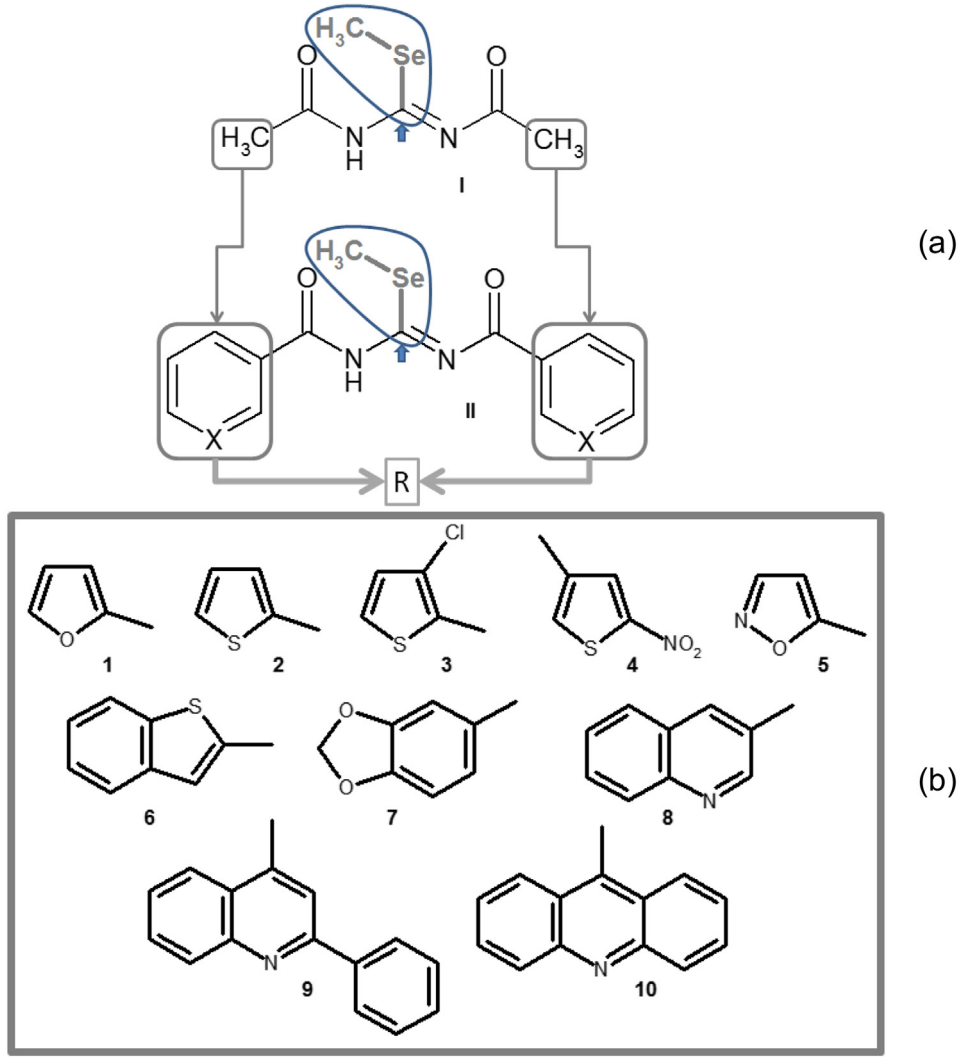

Fig. 1. (a) Structural variations for the first design cycle. Solid arrow indicates the suggested hydrolysis point. (b) Structural overview of the analysed compounds corresponding to the second design cycle.

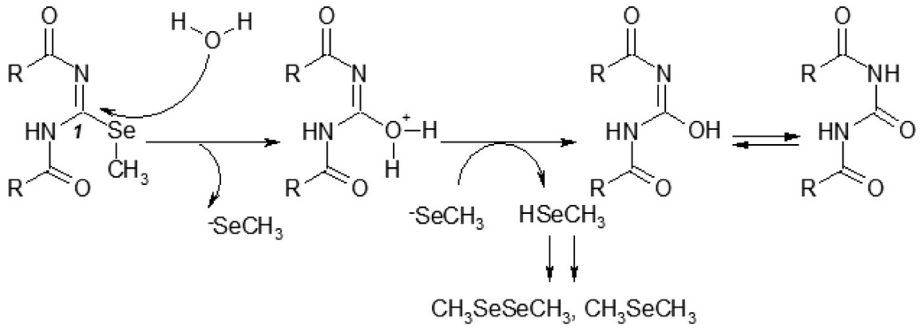

Fig. 2. Proposed mechanism for the MeSeH release.

in colon (HT-29) and breast adenocarcinoma (MCF-7) cell lines and the results are given in Table 1.

The work described here had three main goals. Firstly, the release of the proposed active agent, MeSeH, was verified by applying a screening method supported by analytical techniques, i.e., Head Space Gas Chromatography Mass Spectrometry (HS-GC–MS) [28]. This analysis provided direct identification of the highly volatile, unstable and reactive key compound MeSeH and its recombination products, which include dimethyldiselenide (DiMeDiSe) and dimethylselenide (DiMeSe) according to our previous study [27]. The second goal was to study the conformational behaviour of the molecules in order to evaluate the influence of this factor on the accessibility of the hydrolysis point. The third goal was the application of molecular modelling approaches in order to obtain descriptors, preferably topological and quantum descriptors [26], that would allow us to correlate the molecular structural variations with the hydrolysis of the MeSeH moiety and subsequently with the cytotoxic activity.

The HS-GC–MS data were obtained on an Agilent 6890 GC system coupled to a 5973N quadrupole mass spectrometer (Agilent Technologies, Santa Clara, CA, USA). The compounds were dissolved in 5% dimethylsulfoxide in H_2O (5% DMSO/H_2O) at a concentration of 60 mM. The samples were kept at room temperature in sealed HS-GC–MS vials and samples for analysis were taken from the vial head space at 8, 16 and 24 h for each of the studied BSeCs. Evidence for the positive release of MeSeH was obtained by direct detection of this compound as well through the detection of the secondary recombination compounds DiMeDiSe and DiMeSe [29,30].

Table 1
Average GI_{50}[a] values (μM) for analysed compounds.

Ref.	HT-29[b]	MCF-7[c]
1b	5×10^{-5}	0.03
2b	3.4×10^{-4}	0.0034
3b	0.0049	0.30
4b	6.3×10^{-4}	7.6×10^{-4}
5b	7.9×10^{-4}	9×10^{-5}
6b	5.62	5.07
7b	0.53	0.99
8b	0.20	0.66
9b	0.46	0.49
10b	7.63	73.92
Doxorubicin[d]	0.20	0.02
Camptothecin[d]	0.05	0.01
Etoposide[d]	31.62	19.95
Taxol[d]	0.003	0.003
Cisplatin[d]	7.95	3.16
Methotrexate[d]	0.04	0.06

[a] Concentration that inhibits 50% of cell growth.
[b] Colon carcinoma.
[c] Breast adenocarcinoma.
[d] NCI data (http://dtp.nci.nih.gov).

The molecular modelling calculations were performed on a Dell Precision 380 workstation provided with the software package MOE [31] and on an SGI Virtu VS100 workstation provided with the MOPAC2009 software package [32].

In order to facilitate the understanding of the results concerning the effect of the structural modifications on the target activity, the previously reported analytical and spectroscopic data as well as the activity data and a description of the biological methods are included as supplementary material. Some representative mass and ^1H and ^{13}C NMR spectra are also included in the supplementary on line material.

2. Results and discussion

The architecture of the analysed compounds can be considered as consisting of a methyl carbamimidoselenoate scaffold decorated with a series of different monocyclic, bicyclic and tricyclic aryl or heteroaryl planar rings. These units are connected through a carbonyl fragment on the nitrogen atoms of the scaffold; the structural variations were selected with the aim of evaluating their ability to modulate the release of MeSeH.

The high volatility and reactivity of MeSeH means that its effective release from the analysed BSeCs must be established through the detection of either the compound itself or of any secondary products (DiMeDiSe and DiMeSe) that may appear due to oxidation of the initially released MeSeH and subsequent recombination of the oxidized sub-products. Therefore, in order to standardise the analytical procedure, we first determined the HS-GC–MS behaviour of MeSeH generated *in situ* by reductive hydrolysis with $NaBH_4$ of a solution of commercial DiMeDiSe in methanol.

The data obtained show that hydrolysis is caused by $NaBH_4$ and that a significant amount of MeSeH is detected. This compound subsequently undergoes a progressive oxidative process, which results in the regeneration of the initial compound DiMeDiSe [28]. In fact, two significant peaks were detected when the HS-GC-MS is obtained in SCAN mode: the first peak, with a retention time (t_R) of 1.5 min, corresponds the *in situ* generated MeSeH, whereas the second peak, with a tR of 2.9 min, corresponds to the regenerated DiMeDiSe. The mass spectrum corresponding to each of the peaks are consistent with the expected compounds MeSeH and DiMeDiSe (See representative figures in the supplementary on line material).

Once the mass spectra had been obtained in SCAN mode, the mass detector was operated in SIM mode. The most abundant fragment ions were selected for each standard, according to the characteristic Se isotope patterns of compounds containing one or two Se atoms, and their relative intensities. As a result, *m*/*z* values of 96, 95, 93 and 80 for MeSeH and 190, 188, 186, 175 and 160 for DiMeDiSe were monitored (See representative figure in the supplementary on line material).

Table 2
DMeDSe amount (t_R (min) = 2.897) obtained after 16 and 24 h, for representative compounds (expressed as area).

Ref.	16 h	24 h
1b	23584	29333
2b	16164	23196
8b	15036	23982
10b	12254	18425

The BSeC samples were dissolved in 5% DMSO/H_2O and were stored at room temperature in sealed vials. These samples show interesting behaviour in the same analytical procedure. The data corresponding to the first sampling, taken after 8 h of incubation (data not shown for the sake of brevity), show that compounds **1b** and **3b** undergo the expected hydrolysis, with two intense peaks due to DiMeDiSe and MeSeH. Compound **4b** only gave rise to the MeSeH peak as a trace component. Compounds **2b** and **5b** showed only the DiMeDiSe peak and this had a medium intensity compared to those of **1b** and **3b**. Peaks were not detected for the other compounds tested.

To further study the release kinetics, data were obtained after incubation for 16 and 24 h for four of the compounds, **1b**, **2b**, **8b** and **10b**, which were selected as being representative of the different behaviours in the biological activity.

The areas obtained for the DiMeDiMe generated after incubation for the indicated times (16 and 24 h) are shown in Table 2. The results indicate a greater MeSeH release rate for **1b**. Thus, after an incubation period of 16 h, the amount of DiMeSeMe released by compound **1b** was 45.9% greater than that from compound **2b**, 56.8% greater than that from compound **8b** and 92.46% greater than that from compound **10b**. After 24 h the release rate was similar for all compounds under investigation (See representative figure in the supplementary on line material).

On the basis of the data obtained from this analysis, an initial correlation between the structure of the compounds and the MeSeH release kinetics can be established. In the case of BSeC derivatives that contain monocyclic rings on the scaffold, the release of the active agent is more rapid and has a higher intensity than for the bi- or tricyclic derivatives. This behaviour correlates with biological activity (Table 1) as the most active compounds, especially in the HT-29 cell line (pGI50 = 7.3010, 6.4685, 6.2007, 6.1024 and 5.3098 for compounds **1b**, **2b**, **4b**, **5b** and **3b**, respectively), showed greater ability to liberate the selenomethyl moiety. Similar behaviour was found for the MCF-7 cell line, for which BSeCs **2b**, **4b** and **5b** showed the highest activity.

The activity data allowed us to propose that the cytotoxic capacity could also be related to the different sensitivities of cell lines to the active agent MeSeH. The release rate may also have an influence, as a slow release rate would, in principle, allow the released MeSeH to undergo a more gradual oxidation, thus leading to a higher proportion of DiMeDiSe, which has no direct activity as a cytotoxic agent. A rapid and intense release would lead to a more direct and immediate cytotoxic activity.

In order to gain an insight into the structure–activity relationships that would allow us to explain the results, two different approaches were used to establish a preliminary SAR. Firstly, we analysed the possible influence that structural variations carried out on the BSeC derivatives have on the conformational behaviour. This was achieved by determining the preferred conformation (lowest energy conformation, considered as the global minimum) and subsequent evaluation of the accessibility to the proposed hydrolysis point, i.e. the carbon attached to the selenomethyl fragment (Fig. 1a). This evaluation was carried out using an O2H probe interaction map and by considering the hydrogen bond acceptor/donor map around the hydrolysis point. The second goal was to determine quantitative parameters, preferably topological and quantum parameters, which would allow us to establish a new data set to aid the further design of new molecular entities with improved activity profiles.

The three-dimensional models of the studied compounds were constructed according to three initial basic conformations (Fig. 3a–c) in the vacuum phase (see experimental section for details) and, after a preliminary optimization, the models were subjected to a conformational search (systematic search strategy). This process gave the conformational trajectory (maximum number of lowest energy conformations = 100) for each analysed compound (Fig. 3d).

The final conformations obtained for each compound were distributed into two conformational families named 'folded' and 'extended'. The 'folded' family includes the conformations that have a more globular architecture, frequently with the lateral rings involved in pi–pi stacking interactions (preferably T-shaped or sandwich), whereas the 'extended' family includes the conformations that fit an extended molecular architecture. Several representative conformations are shown in Fig. 4 and these illustrate the results of the conformational analysis.

It can be deduced from the data collected in Table 3 that the BSeCs with lateral monocyclic rings showed a preference for extended conformations, especially for compounds that were unsubstituted at the rings. For example, compound **1b** only gave rise to extended-type conformations; similar behaviour was found for compounds **2b** and **5b**, both of which showed a significant preference for the extended conformation. Although compounds **3b** and **4b** also show a clear preference for the extended form, appreciable amounts of folded forms were evident due to the interactions established by the substituents on the rings. It can also be observed that as the molecular architecture becomes more complex, i.e. on increasing the size of the lateral rings from monocyclic to bi- and tricyclic, the proportion of folded conformations progressively increases and the aforementioned interactions are detected between the rings.

These data allow us to establish a clear relationship between the preferred conformation shown by the analysed BSeCs and their ability to release MeSeH. As can be observed, the compounds for which the determined release was faster and more intense (e.g. compound **1b**) preferentially adopt an extended conformation, whereas compounds such as **10b**, for which the release of MeSeH was very slow and minor, the folded conformation was preferred.

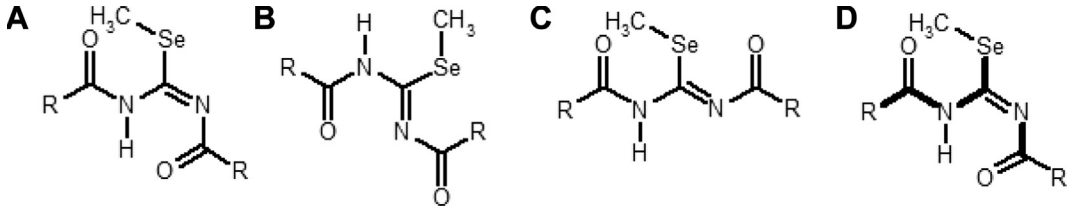

Fig. 3. Initial conformations taken as a starting point for the conformational analysis. Solid line, selected rotatable bonds.

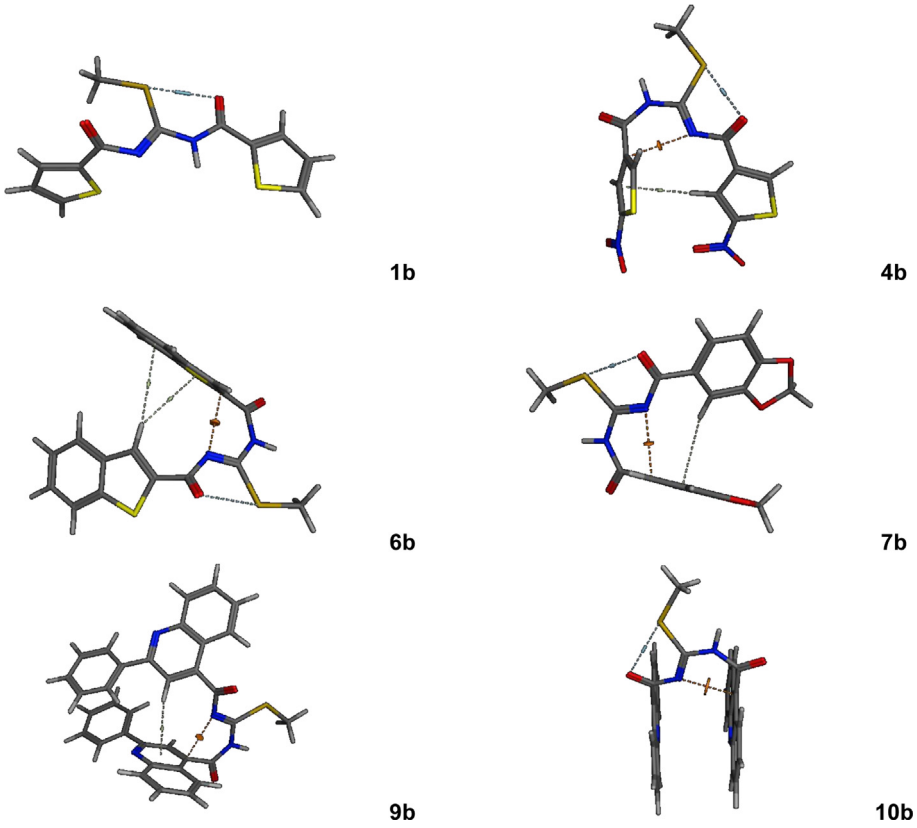

Fig. 4. Representative folded and extended conformations. Dotted lines indicate the detected clashes.

Compounds with an intermediate release, such as **8b**, showed conformational behaviour that was distributed between the folded and extended families.

The lowest energy conformations for compounds **1b**, **2b**, **3b**, **4b**, **5b** and **8b** are included in the extended conformational family, while those for **6b**, **7b**, **9b** and **10b** are included in the folded family (see Fig. 4 for representative examples).

Table 3
Conformational distribution for the analysed compounds.

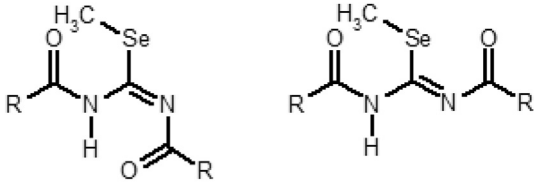

Ref.	% Folded	% Extended
1b	0	100
2b	8	92
3b	28	72
4b	39	61
5b	16	84
6b	32	68
7b	42	58
8b	45	55
9b	95	5
10b	98	2

It can be concluded from this initial study that in the extended conformations the hydrolysis point is more exposed to attack by the nucleophile than in the folded forms, a situation that results in an increased release of MeSeH.

In order to confirm the above conclusion, the interaction map of the molecular surface was also calculated for each compound by employing an O2H probe (0.00 charge, with an interaction energy of −5.5 kcal/mol). The graphical representation showing where this chemical probe has favourable interactions with the molecular surface, calculated according to Goodford's GRID approach [33], confirms that the more favourable interactions were shown by compounds **1b**, **2b**, **4b** and **5b** (see Figs. 5 and 6 for representative examples). In these cases the interaction map is located close to the C that bears the selenomethyl moiety, i.e., the proposed hydrolysis point.

It can be observed in Fig. 6 that the folded compounds, such as **9b** or **10b**, have an interaction map that is located far from the hydrolysis point.

With respect to the second molecular modelling approach, we calculated a significant number of 2D and 3D molecular descriptors (see supplementary material for details) with the aim of establishing the parameters that could aid the design of new series' of compounds with the target activity.

Data obtained in the first design cycle were used to select the calculated descriptors. These descriptors were subsequently applied in the design of the BSeCs analysed here according to the bond order between Se and the carrier carbon (Fig. 1). The bond order (b.o.) should be as low as possible and the LUMO and HOMO orbitals should preferably be located on the scaffold atoms. The data obtained for the currently analysed BSeCs, which concern the accessibility of the hydrolysis point and the interaction between the O2H probe and acceptor/donor maps, were also considered when

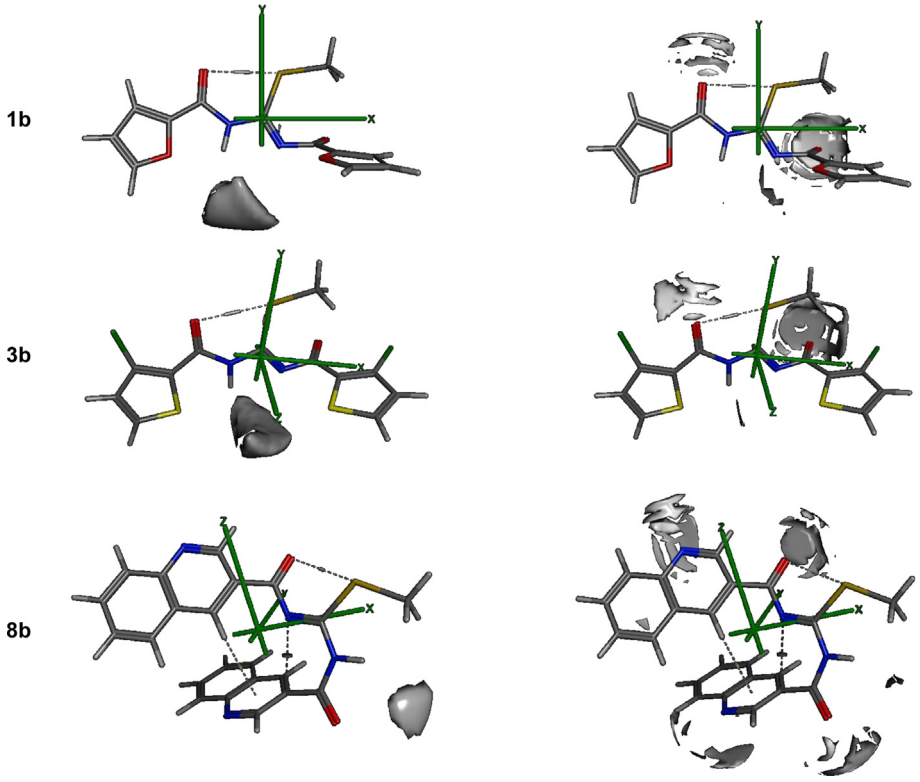

Fig. 5. Left; interaction map (O2H probe, −5.5 kcal/mol contour value); right, acceptor/donor interaction map (−2 kcal/mol contour value) for **1b** and **3b**, as examples of extended compounds showing a faster and more intense MeSeH release, and **8b**, as an example of a folded compound with medium release rate (calculated on the lowest energy conformations).

selecting which parameters to estimate. Thus, as an initial approach the calculated descriptors can be grouped as follows: (a) Topological information indices (Adjacency and Distance Matrix Descriptors): BalabanJ [34] (as a topostructural descriptor) and BCUT_PEOE [35] (as a topochemical descriptor). (b) Quantum_chemical descriptors: PM3-Q_{Se} (Se partial charge); PM3-Q_{C1} (C1 partial charge); b.o. (bond order C1–Se); PM3-EHOMO (HOMO orbital energy and location); PM3-ELUMO (LUMO orbital energy and location);

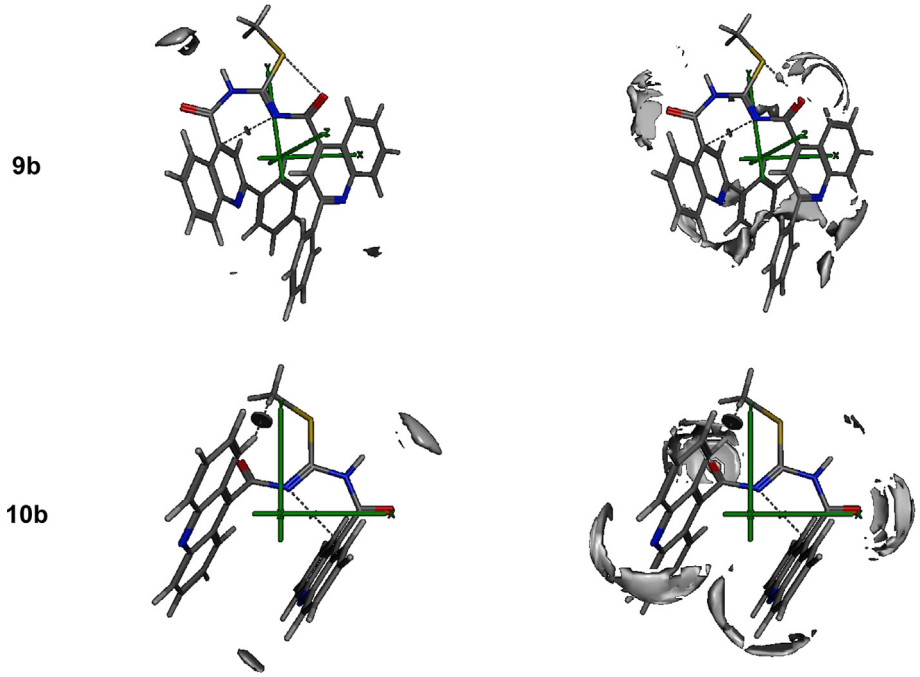

Fig. 6. Left; interaction map (O2H probe, −5.5 kcal/mol contour value); right, acceptor/donor interaction map (−2 kcal/mol contour value) for compounds **9b** and **10b**, as examples of folded compounds with low or null release of MeSeH (calculated on the lowest energy conformations).

PM3-dipole. (c) Physical properties and hydrophobicity descriptors: logP (o/w) and SlogP (log of the octanol/water partition), logS (log of the aqueous solubility), vdw_vol and vdw_area (van der Waals volume and area calculated using a connection approximation). (d) Surface Area, volume and shape descriptors: ASA (water accessible surface area); vol and VSA (van der Waals volume and area calculated using a grid approximation); vsuf_V and vsurf_S (interaction field volume and area). (e) Conformation dependent charge descriptors and partial charge descriptors: ASA+ (water accessible surface area of all atoms with positive partial charge); ASA− (Water accessible surface area of all atoms with negative partial charge); ASA_H (water accessible surface area of all hydrophobic atoms); ASA_P (water accessible surface area of all polar atoms); PEOE_VSA_NEG (Total negative van der Waals surface area); PEOE_VSA_POS (Total positive van der Waals surface area) [36]. In this way it was intended to assess topological, hydrophobic and electrostatic aspects. The final values used for the conformationally dependent parameters, as well as for the quantum descriptors, were the mean values obtained for the conformational trajectory (see supplementary material).

The small number of compounds that comprise this series and the high number of analysed parameters required us to perform an initial Principal Components Analysis and a subsequent contingency and correlation analysis [37] (data not shown for the sake of brevity). This process allowed us to detect those descriptors that are likely to be more important in establishing structure-activity relationships.

The selected descriptors, i.e., those for which we obtained the best correlation values, are shown in Table 4.

The data concerning the atomic charges for Se and C scaffold atoms and the Se–C b.o. are included for comparative purposes [26]. It is necessary to bear in mind that the structural modifications proposed in the design cycle that gave rise to the present derivatives were carried out using a selection of rings chosen prior to assessing the later parameters. Structures were chosen that had a b.o. between 0.8320 and 0.9061, with the exceptions being compound **5b**, with a mean b.o. of 0.9449, and compound **6b**, with a mean b.o. of 0.9539. However, **5b** was active in both cell lines whereas **6b**, as expected, was inactive. These results, along with the MeSeH release data discussed previously, allowed us to confirm our starting hypothesis, according to which a lower b.o. value implies a more probable and effective release of the active agent.

The energy and location of the frontier orbitals (HOMO 0 and LUMO 0) were calculated by applying the PM3 Hamiltonian included in the Mopac software. As a general trend, higher values for the HOMO orbital were obtained for the inactive compounds **6b** and **10b**. The preferred location for this orbital in the active compounds is in the central molecular fragment, whereas for the inactive compounds the location is displaced towards one of the lateral rings. Regarding the LUMO orbital, as a general trend this frontier orbital is also located on the central fragment of the molecule in the active compounds, with a significant contribution from the C atom proposed as the hydrolysis point; a lower contribution from this atom to the LUMO orbital was observed for the inactive BSeCs (see Fig. 7 for representative examples).

A clear relationship can be established between the topology, evaluated through the BalabanJ index, and the cytotoxic activity. In fact, the most active compounds have a BalabanJ value in the range 1.7556–1.8230, whereas the inactive compounds (e.g. **9b** and **10b**) have a value below 1.200.

With respect to the data obtained for the HT-29 cell line, it can be observed that the ASA descriptor (water accessible surface area calculated using a radius of 1.4 Å for the water molecule) shows a significant relationship with the cytotoxic activity, with the most active compounds having the lowest ASA values. These data can be misleading as one would expect that a larger surface exposed to water, the nucleophile responsible for hydrolysis in the proposed mechanism, would lead to greater accessibility to the attack point. However, analysis of the data, together with the O2H probe interaction map described above, led us to propose that the exposed surface is smaller for the most active compounds but is located close to the aforementioned attack point. The ASA + descriptor, which represents the water accessible surface area of all atoms with positive partial charge (strictly greater than 0), showed a similar general trend.

The van der Waals volume (vdw_vol) and area (VSA) values can also be related to the activity. The active compounds **1b**, **2b**, **3b**, **4b** and **5b** have the smallest volumes and areas, with values of less than 406 $Å^3$ for the van der Waals volume (calculated using a connection table approach) and 352 $Å^2$ for the VSA descriptor.

With respect to the data obtained for the MCF-7 cell line, it can be observed that the ASA-H descriptor (water accessible surface area of all hydrophobic atoms) shows a clear relationship with the cytotoxic activity. In fact, the most active compounds in this cell line (**1b**, **2b**, **3b**, **4b** and **5b**) have significantly lower values than the inactive compounds.

In a similar way, the PEOE_VSA_HYD descriptor, which quantifies the total hydrophobic van der Waals surface area based on the

Table 4
Selected descriptors.

Ref	pGI_{50} HT-29	pGI_{50} MCF-7	Q_{Se}[a]	Q_{C1}[a]	b.o.	E_{HOMO}[b]	BalabanJ	ASA[c]	ASA_H[c]	PEOE_VSA_HYD[c]	vdw_vol[d]	VSA[c]
1b	7.3010	4.5229	0.089	−0.117	0.84854	−9.1990	1.7556	498.4686	375.7461	210.3316	334.4484	285.5584
2b	6.4685	5.4685	0.093	−0.110	0.83242	−9.1283	1.7556	518.7032	305.7778	232.7572	357.8914	303.7578
3b	5.3098	4.4318	0.092	−0.108	0.83248	−9.0205	1.8230	546.5300	346.8099	267.9200	389.8033	334.6382
4b	6.2007	6.1192	0.132	−0.116	0.84612	−9.7555	1.7836	578.4913	196.4080	164.2993	405.6955	351.2402
5b	6.1024	6.0458	0.106	−0.128	0.94485	−9.5459	1.7556	482.0561	392.7048	178.6266	314.0371	273.8548
6b	2.2503	2.2950	0.093	−0.114	0.95391	−8.9056	1.2516	645.5012	481.5653	307.6725	501.9259	398.3111
7b	3.2757	3.0044	0.171	−0.104	0.89594	−9.1083	1.2467	607.7132	481.1737	278.6299	462.7507	368.6017
8b	3.6990	3.1805	0.057	−0.128	0.90659	−9.2277	1.2429	660.4120	575.5024	311.2517	524.9222	406.3987
9b	3.3372	3.3098	0.0520	−0.126	0.87491	−9.03321	1.0986	857.7306	789.5089	452.2481	754.8700	564.9666
10b	2.1175	1.1312	0.1220	−0.113	0.85379	−8.68594	1.1499	730.5948	665.9265	386.1669	668.9567	495.2197
R^2[e]						0.4372	0.8308	0.5763	0.5497	0.6074	0.6168	0.5877
R^2[f]						0.7177	0.7377	0.4528	0.5679	0.6210	0.5365	0.4841

[a] Coulson type charges.
[b] in eV, average value for the lowest energy conformers for each analysed compound.
[c] in $Å^2$.
[d] in $Å^3$.
[e] R^2 correlation coefficient for HT-29 cytotoxicity assay.
[f] R^2 correlation coefficient for MCF-7 cytotoxicity assay.

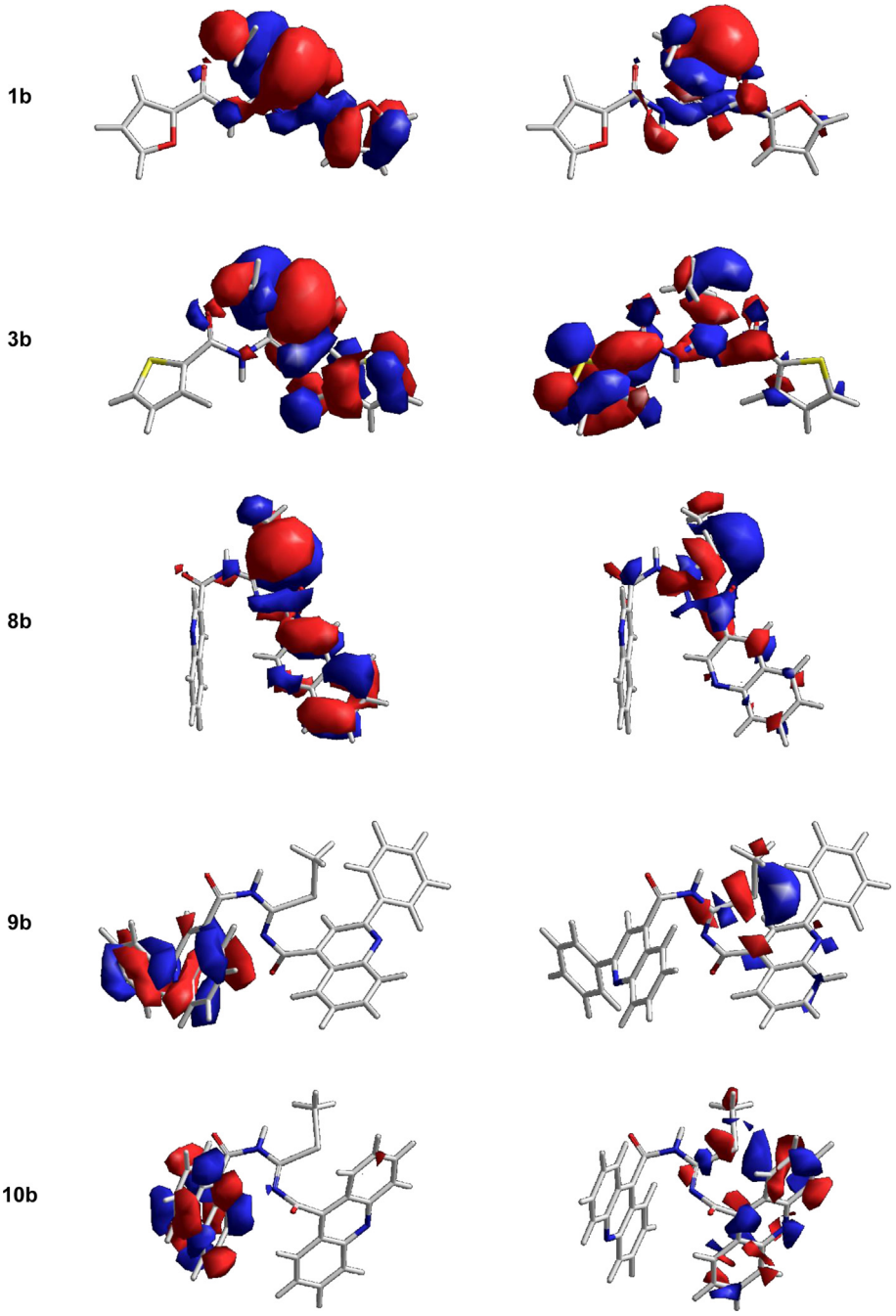

Fig. 7. Orbital distribution (left: HOMO 0; right: LUMO 0) for representative active and inactive compounds (representative lowest energy conformation).

Partial Equalization of Orbital Electronegativities (PEOE) [37] method to calculate the atomic partial charges, can be related to the activity in both cell lines. In this case, the most active compounds (**1b**, **2b**, **4b** and **5b**) have lower values than the inactive ones.

3. Conclusions

The data obtained in this study confirmed our initial hypothesis and allowed us to establish a preliminary correlation between the structure of the compounds, their conformational behaviour, the MeSeH release kinetics and the biological activity. In fact, for active compounds such as **1b**, **2b**, **4b** or **5b** we have demonstrated, by means of HS-GC–MS techniques, their ability to release the proposed active cytotoxic agent MeSeH. Furthermore, a common preference for the extended-type conformation has been highlighted and this structural arrangement facilitates access of the nucleophilic agent, which causes the release of the selenomethyl moiety. An O2H probe interaction map supports this conclusion.

The molecular topology, evaluated through the BalabanJ index, has a significant relationship with the target activity. For the most active compounds the BalabanJ index has values between 1.7556 and 1.8230, whereas the inactive compounds have a significantly lower BalabanJ value.

Another structural characteristic is the preferred location of the frontier HOMO and LUMO orbitals and this can also be related to

the cytotoxic activity. In the active compounds the orbital is located over the scaffold moiety whereas in the inactive compounds the orbital is displaced to one of the lateral heteroaryl rings.

The data presented in this paper are currently being used in a new design cycle for the development of novel compounds that can modulate the release of MeSeH through successive structural variations. The structural changes concern the molecular environment surrounding the hydrolysis site and encourage a bias towards extended conformations and a topology consistent with the data obtained in the present study. In this approach the whole molecule is considered as a pro-drug and the selected structural variations represent the release regulator elements.

4. Experimental

4.1. Head Space Gas Chromatography Mass Spectrometry (HS-GC–MS) analysis

HS-GC–MS was performed as described in the literature [28]. DiMeDiSe and MeSeH were used as standards. DiMeDiSe (Sigma, St. Louis, MO, USA) was dissolved in methanol as a stock solution (10 mM). MeSeH was generated *in situ* by reductive hydrolysis induced by $NaBH_4$ (Sigma, St. Louis, MO, USA) in HS-GC–MS vials: 2.4 μL of DiMeDiSe was dissolved in 1 mL of ethanol and 20 mg $NaBH_4$ was added. The vial was capped using a rubber septum with a crimp cap.

The analysed compounds were prepared in the same vials by dissolving a sample in 5% DMSO/H_2O at a final concentration of 60 mM. The vial was capped as before and the mixture was kept at room temperature. The analytical samples were taken from the head space at 8, 16 and 24 h.

Chromatographic analyses were carried out on an Agilent 6890 gas chromatograph coupled to a 5973N quadrupole mass spectrometer (Agilent Technologies, Santa Clara, CA, USA). An HP-5MS capillary column (30 m × 0.25 mm I.D.) coated with a 0.25 μm film of stationary phase (5% phenyl methylsiloxane) was used. The flow rate of the high purity helium carrier gas was 1 mL/min. The split/split less inlet was operated in split mode, with a 50:1 split ratio. The injector was held at 250 °C and the transfer line to the detector at 300 °C.

The GC oven temperature was 60 °C, isothermal for 1 min, 50 °C × min^{-1} to 140 °C, then 1 min isothermal. The MS was operated in electron impact mode (EI, 70 eV).

The GC/MS was first operated in SCAN mode to determine the selected ion monitoring (SIM) parameters for the expected volatile species DiMeDiSe and MeSeH; once these parameters had been established, the GC/MS was operated in SIM mode, establishing the conditions through the selection of the most abundant fragment ions of standards and the relative intensity of each one, according the characteristic Se isotope patterns of compounds containing one or two Se isotopes. Thus, the SIM conditions were established for MeSeH (*m*/*z* 80, 93, 95 and 96) and for DiMeDiSe (*m*/*z* 190, 188, 186, 175 and 160).

4.2. Molecular modelling methods

The calculations were performed on a Dell Precision 380 workstation, provided with the software package MOE [31], and on an SGI Virtu VS100 workstation, provided with MOPAC2009 [32] software package.

The three-dimensional models of the studied compounds were constructed according to three initial basic conformations in the vacuum phase, using atoms and structural fragments from the Builder module (MOE2012.10) and using the implemented MMFF94x [38] force field. A preliminary optimization was carried out by applying the implemented Energy Minimize general strategy with a root mean square gradient, rms of 0.001 kcal/mol/Å^2 as completion criterion. Restraints and constraints were not applied. The first minimized conformations obtained were considered as the starting conformations for the conformational analysis.

The conformational search was carried out through a systematic search strategy with an rms gradient of 0.001 kcal/mol/Å^2, an energy window of 5 kcal and a maximum conformation number of 100. The resulting conformations were then optimized by applying the MOPAC2009 engine, using the PM3 semi-empirical approach, with the geometry optimized using an eigenvector following algorithm (rms gradient of 0.001 kcal/mol/Å^2).

The resulting conformations for each compound were distributed into two families ('folded' and 'extended'), with the distribution criterion taken as the maximum distance between the geometric centres of the extreme rings.

The Interaction Potentials map that predicts the preferred location of an O2H probe was calculated for the lowest energy conformation by applying the calculation method implemented in the MOE2012.10 software suite, which is based on a force field that incorporates van der Waals, charge and hydrogen bonding terms. The contour map represents the interaction energy equal to −5.5 kcal/mol.

The Electrostatic Feature Maps that predict the electrostatically preferred locations of H-bond acceptor and H-bond donor sites from the solutions of the Poisson–Boltzmann equation were calculated over the representative lowest conformation selected for each analysed BSeC by applying the calculation method implemented in the MOE2012.10 software suite. The contour map represents the interaction energy equal to −2 kcal/mol.

The calculated 2D and 3D descriptors (see supplementary material for details) were selected from those available in the MOE2012.10 suite, which is intended to cover a wide range of both physical and topological properties as well as electrostatic and quantum characteristics.

The value collected for the conformationally dependent descriptors represents the average value calculated for all conformations of each compound.

In order to reduce the dimensionality of the set of selected molecular descriptors, a Principal Components Analysis (PCA) was applied, with a component limit equal to 3 and 80% of minimum variance. A further contingence analysis was carried out on the aforementioned descriptor set.

The atomic charges (Coulson type charges [39]) and the bond orders were calculated by applying the PM3 semi-empirical approach. The data collected represent the average values for the conformations obtained. The locations of HOMO and LUMO orbitals were calculated on the lowest energy conformation.

Appendix A. Supplementary data

Supplementary data related to this article can be found at http://dx.doi.org/10.1016/j.ejmech.2013.06.001.

References

[1] P.D. Whanger, Selenium and its relationship to cancer: an update, Br. J. Nutr. 91 (2004) 11–28.
[2] M.P. Rayman, Food-chain selenium and human health: emphasis on intake, Br. J. Nutr. 100 (2008) 254–268.
[3] M.P. Rayman, Selenium in cancer prevention: a review of the evidence and mechanism of action, Proc. Nutr. Soc. 64 (2005) 527–542.
[4] H. Zeng, G.F. Combs Jr., Selenium as an anticancer nutrient: roles in cell proliferation and tumor cell invasion, J. Nutr. Biochem. 19 (2008) 1–7.
[5] J. Lü, C. Jiang, Selenium and cancer chemoprevention: hypotheses integrating the actions of selenoproteins and selenium metabolites in epithelial and non-epithelial target cells, Antioxid. Redox Signal 7 (2005) 1715–1727.

[6] A.F. Amaral, K.P. Cantor, D.T. Silverman, N. Malats, Selenium and bladder cancer risk: a meta-analysis, Cancer Epidemiol. Biomarkers Prev. 19 (2010) 2407–2415.
[7] B.K. Dunn, E.S. Richmond, L.M. Minasian, A.M. Ryan, L.G. Ford, A nutrient approach to prostate cancer prevention: the Selenium and Vitamin E Cancer Prevention Trial (SELECT), Nutr. Cancer 62 (2010) 896–918.
[8] M.S. Stratton, A.M. Algotar, J. Ranger-Moore, S.P. Stratton, E.H. Slate, C.-H. Hsu, P.A. Thompson, L.C. Clark, F.R. Ahmann, Oral selenium supplementation has no effect on prostate-specific antigen velocity in men undergoing active surveillance for localized prostate cancer, Cancer Prev. Res. 3 (2010) 1035–1043.
[9] A.M. Algotar, M.S. Stratton, F.R. Ahmann, J. Ranger-Moore, R.B. Nagle, P.A. Thompson, E. Slate, C.H. Hsu, B.L. Dalkin, P. Sindhwani, M.A. Holmes, J.A. Tuckey, D.L. Graham, H.L. Parnes, L.C. Clark, S.P. Stratton, Phase 3 clinical trial investigating the effect of selenium supplementation in men at high-risk for prostate cancer, Prostate 73 (2013) 328–335.
[10] K. El-Bayoumy, The negative results of the select study do not necessarily discredit the selenium-cancer prevention hypothesis, Nutr. Cancer 61 (2009) 285–286.
[11] J.L. Barger, T. Kayo, T.D. Pugh, J.A. Vann, R. Power, K. Dawson, R. Weindruch, T.A. Prolla, Gene expression profiling reveals differential effects of sodium selenite, selenomethionine, and yeast-derived selenium in the mouse, Genes Nutr. 7 (2012) 155–165.
[12] M. Suzuki, M. Endo, F. Shinohara, S. Echigo, H. Rikiishi, Differential apoptotic response of human cancer cells to organoselenium compounds, Cancer Chemother. Pharmacol. 66 (2010) 475–484.
[13] A. Bhattacharya, Methylselenocysteine: a promising antiangiogenic agent for overcoming drug delivery barriers in solid malignancies for therapeutic synergy with anticancer drugs, Expert Opin. Drug Del. 8 (2011) 749–763.
[14] K. Lunoe, C. Gabel-Jensen, S. Sturup, L. Andresen, S. Skov, B. Gammelgaard, Investigation of the selenium metabolism in cancer cell lines, Metallomics 3 (2011) 162–168.
[15] H. Infante, S.P. Joel, E. Warburton, C. Hopley, R. Hearn, S. Jüliger, Investigation of the selenium species distribution in a human B-cell lymphoma line by HPLC- and GC-ICP-MS in combination with HPLCESIMS/MS and GC-TOFMS after incubation with methylseleninic acid, J. Anal. At. Spectrom. 22 (2007) 888–896.
[16] S. Cuello, S. Ramos, R. Mateos, M.A. Martin, Y. Madrid, C. Camara, L. Bravo, L. Goya, Selenium methylselenocysteine protects human hepatoma HepG2 cells against oxidative stress induced by tert-butyl hydroperoxide, Anal. Bioanal. Chem. 389 (2007) 2167–2178.
[17] H. Zeng, M. Briske-Anderson, M. Wu, M.P. Moyer, Methylselenol, a selenium metabolite, plays common and different roles in cancerous colon HCT116 cell and noncancerous NCM460 colon cell proliferation, Nutr. Cancer 64 (2012) 128–135.
[18] J. Lu, C. Jiang, Selenium and cancer chemoprevention, Antioxid. Redox Signal 7 (2005) 1715–1727.
[19] C. Ip, H. Thompson, Z. Zhu, H. Ganther, In vitro and in vivo studies of methylseleninic acid: evidence that a monomethylated selenium metabolite is critical for cancer chemoprevention, Cancer Res. 60 (2000) 2882–2886.
[20] Z. Wang, C. Jiang, J. Lu, Induction of caspase-mediated apoptosis and cell-cycle G1 arrest by selenium metabolite methylselenol, Mol. Carcinog. 34 (2002) 113–120.
[21] H. Zeng, M. Wu, J.H. Botnen, Methylselenol, a selenium metabolite, induces cell cycle arrest in G1 phase and apoptosis via the extracellular-regulated kinase 1/2 pathway and other cancer signaling genes, J. Nutr. 139 (2009) 1613–1618.
[22] H. Zeng, M. Briske-Anderson, J.P. Idso, C.D. Hunt, The selenium metabolite methylselenol inhibits the migration and invasion potential of HT1080 tumor cells, J. Nutr. 136 (2006) 1528–1532.
[23] R. Zhao, F.E. Domann, W. Zhong, Apoptosis induced by selenomethionine and methioninase is superoxide mediated and p53 dependent in human prostate cancer cells, Mol. Cancer Ther. 5 (2006) 3275–3284.
[24] E. Ibáñez, D. Plano, M. Font, A. Calvo, C. Prior, J.A. Palop, C. Sanmartín, Synthesis and antiproliferative activity of novel symmetrical alkylthio- and alkylseleno-imidocarbamates, Eur. J. Med. Chem. 46 (2011) 265–274.
[25] E. Ibáñez, A. Agliano, C. Prior, P. Nguewa, M. Redrado, I. Gonzalez-Zubeldia, D. Plano, J.A. Palop, C. Sanmartín, A. Calvo, The quinoline imidoselenocarbamate EI201 blocks the AKT/mTOR pathway and targets cancer stem cells leading to a strong antitumor activity, Curr. Med. Chem. 19 (2012) 3031–3043.
[26] M. Font, A. Zuazo, E. Ansó, D. Plano, C. Sanmartín, J.A. Palop, J.J. Martínez-Irujo, Novel structural insights for imidoselenocarbamates with antitumoral activity related to their ability to generate methylselenol, Bioorg. Med. Chem. 20 (2012) 5110–5116.
[27] A. Zuazo, D. Plano, E. Anso, E. Lizarraga, M. Font, J.J. Martínez-Irujo, Cytotoxic and proapototic activities of imidoselenocarbamate derivatives are dependent on the release of methylselenol, Chem. Res. Toxicol. 25 (2012) 2479–2489.
[28] C. Gabel-Jensen, K. Lunoe, B. Gammelgaard, Formation of methylselenol, dimethylselenide and dimethyldiselenide in in vitro metabolism models determined by headspace GC-MS, Metallomics 2 (2010) 167–173.
[29] C.M. Weekley, J.B. Aitken, S. Vogt, L.A. Finney, D.J. Paterson, M.D. de Jonge, D.L. Howard, I.F. Musgrave, H.H. Harris, Uptake, distribution, and speciation of selenoamino acids by human cancer cells: X-ray absorption and fluorescence methods, Biochemistry-US 50 (2011) 1641–1650.
[30] C.M. Weekley, J.B. Aitken, I.F. Musgrave, H.H. Harris, Methylselenocysteine treatment leads to diselenide formation in human cancer cells: evidence from X-ray absorption spectroscopy studies, Biochemistry-US 51 (2012) 736–738.
[31] *Molecular Operating Environment (MOE)*, 2012.10; Chemical Computing Group Inc., 1010 Sherbooke St. West, Suite #910, Montreal, QC, Canada, H3A 2R7, 2012
[32] MOPAC MOPAC2009 J.P. Stewart, Stewart Computational Chemistry, Colorado Springs, Co, USA, 2009, http://OpenMOPAC.net.
[33] P.J. Goodford, A computational procedure for determining energetically favorable binding sites on biologically important macromolecules, J. Med. Chem. 28 (1985) 849–857.
[34] A.T. Balaban, Highly discriminating distance-based topological index, Chem. Phys. Lett. 89 (1982) 399–404.
[35] R.S. Pearlman, K.M. Smith, Novel software tools for chemical diversity, Persp. Drug Discov. (1998) 339–353, 9/10/11.
[36] J. Gasteiger, M. Marsili, Iterative partial equalization of orbital electronegativity – a rapid access to atomic charges, Tetrahedron 36 (1980) 3219–3228.
[37] R.V. Hogg, E.A. Tanis, Probability and Statistical Inference, Macmillan Publishing, New York, 1993.
[38] T.A. Halgren, MMFF VI. MMFF94s option for energy minimization studies, J. Comput. Chem. 20 (1999) 720–729.
[39] J. Meister, W.H.E. Schwarz, Principal components of ionicity, J. Phys. Chem.-US 98 (1994) 8245–8252.